# Transport Phenomena in Carbon Nanostructures

Toshishige Yamada, Tsutomu Saito, Drazen Fabris, and Cary Y. Yang
Center for Nanostructures, Santa Clara University, Santa Clara, California
Phone: (408) 554-6814 Fax: (408) 554-5474 Email: cyang@scu.edu

***Abstract* – An empirical model is developed that takes into account heat transport through the entire carbon nanofiber interconnect test structure and breakdown location. This electrothermal transport model elucidates observed current capacity behavior, and predicts variations in contact location with the support material. The resulting heat dissipation and current capacity are completely consistent with measurement data.**

## I. INTRODUCTION

CARBON nanostructures have been studied for future interconnect applications due to their immunity to electromigration and excellent electrical and thermal transport properties [1-9]. Carbon nanofiber (CNF) is an allotrope of carbon nanotube (CNT) with a cone-like central core structure and a multilayer outer wall structure (similar to multiwall CNT) [9-10]. But unlike multiwall CNT, CNF does not have a hollow interior. To understand their transport properties as interconnects, we have developed a simple model based on measurements of the maximum current density $J_{max}$ at breakdown [11-12]. Further, an imaging technique has been developed to quantify the observations [13]. Previous work [11] has indicated reasonable convergence of $J_{max}$ data for CNF suspended between two electrodes, while CNF in partial contact with a $SiO_2$ substrate shows larger $J_{max}$ and wider scatter as shown in Fig. 1. Since breakdown has been shown to be associated with the peak CNF temperature [6,14,15], substrate contact should enhance heat dissipation, increase the immunity to Joule heating, and hence increase $J_{max}$. Recently, we have extended the previous model to capture the variation in heat transport to the $SiO_2$ substrate due to partial CNF contact [16]. In addition, we demonstrate the contrast between heat dissipation through two different electrodes and through the substrate.

The new model adds two important parameters. One is the support fraction $S$, defined as the ratio of the length in contact with the $SiO_2$ substrate to the CNF inter-electrode length $L$. $S$ is measurable from a scanning electron microscope (SEM) image, where suspended segments are brighter due to more efficient secondary electron generation [13] as shown in Fig. 2. The other is the spatially varying heat dissipation factor $a(x)$ to describe heat transport from CNF to its environment (air, substrate, or electrode). The values of $a(x)$ are determined by fitting to experimental data.

We use two types of CNF-electrode contacts. For the first type, a CNF is placed on Au electrodes, which are about ~100 nm higher than the $SiO_2$ surface, using a drop-cast technique [11-12]. The initial resistance between the electrodes is in the MΩ range, but after several cycles of applied current (current-stressing), it decreases to the kΩ range [11]. For the second type of contact, a CNF is placed on Au electrodes and then tungsten (W) is deposited to secure the contact [12]. The total resistance is in the kΩ range, and there is little effect from current stressing. $J_{max}$ is consistently larger with W-Au contacts than with Au contacts as shown in Fig. 1.

Breakdown always occurs in the suspended region. There are three cases shown in Fig. 2: 1) For $S = 0$, breakdown occurs at or near the midpoint with W-Au contacts or Au contacts; 2) for $0 < S < 1$ with Au & $SiO_2$ contacts, breakdown occurs near the middle of the suspended segment; and 3) for $0 < S < 1$ with W-Au & $SiO_2$ contacts, breakdown occurs close to the $SiO_2$-supported region. SEM images of breakdown are shown in Figs. 2(a) - (c), corresponding to cases 1) - 3) above.

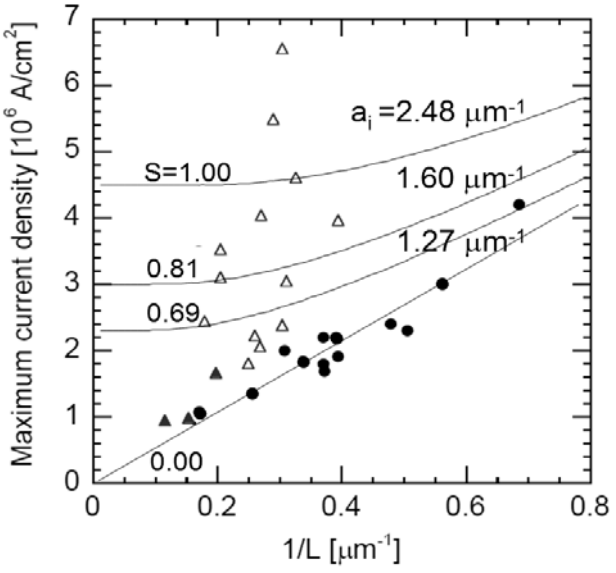


Fig. 1. Measured maximum current density $J_{max}$ as a function of reciprocal CNF length $L$ with different electrodes: suspended CNFs with Au electrodes (solid circles), and suspended (solid triangles) or $SiO_2$-supported (open triangles) CNFs with W-Au electrodes [12]. Lines indicate calculated $J_{max}$ for three fitting values of dissipation factor $a_i$ with $R << 1$. Each line is labeled with the measured fraction of total supported segments $S$.

## II. HEAT TRANSPORT MODEL

To explain these experimental findings, we solve a one-dimensional heat transport equation [5,11,14,16],

$$\frac{d^2\Delta T(x)}{dx^2} - a^2\Delta T = -bJ^2. \qquad (1)$$

$\Delta T$ is the local CNF temperature at $x$ measured from the ambient temperature. $J$ is the current density and $a$ is the dissipation factor measuring the effectiveness of heat dissipation to the contact material with unit of inverse length. $b = 1/(\kappa\sigma)$, where $\kappa$ is the thermal conductivity and $\sigma$ the electrical conductivity of the CNF. Heat diffusion (first term) and heat dissipation (second term) generally depend on location, while heat generation (right hand side) does not. If $a$ is constant, the general solution for Eq. (1) is given by

$$\Delta T(x) = A\cosh(ax) + B\sinh(ax) + bJ^2 , \qquad (2)$$

where $A$ and $B$ are constants determined by boundary conditions. Across the interface between two domains with different dissipation factor $a$, we require that $\Delta T$ and $d\Delta T/dx$ be continuous.

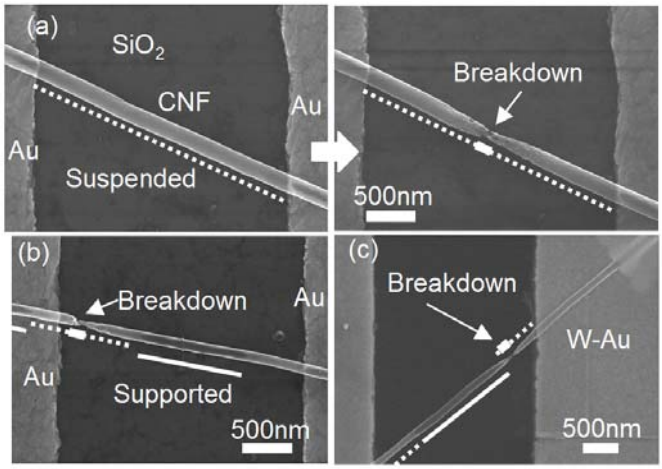


Fig. 2. Breakdown cases, where dotted (solid) lines indicate suspended (supported) segments of a CNF identified through image contrast [13]: (a) Case 1: Au contacts, before (left) and after (right) breakdown at midpoint; (b) Case 2: near-midpoint breakdown with Au & $SiO_2$ contacts. (c) Case 3: breakdown closer to $SiO_2$ side with $SiO_2$ & W-Au contacts. In (b), a suspended segment exists over the electrode region. High-resolution images at a breakdown point were reported in Ref. [10].

### *A. $J_{max}$ as a Function of L for Symmetric Contacts*

Because of symmetry, we consider only the right half of the CNF. As shown in Fig. 3(a), for the electrode region $x \geq L/2$, $a(x) = a_0$, while the region between the electrodes $0 < x < L/2$, $a(x) = a_i$. Since heat dissipation is larger in the electrode region, $R \equiv a_i/a_0 < 1$ holds true. For $J_{max}$ analysis, $a_i$ is appropriately weighted over supported and suspended regions in partially supported cases of $0 < S < 1$. We assume that CNF breakdown occurs when $\Delta T_{max}$ reaches the threshold $\Delta T_{th}$ [11], which is independent of the CNF length or radius. Then it is possible to express $J_{max}$ as a function of $\Delta T_{th}$ , $a_i$, $b$, $R$, $L$, and $J_0(a_i) = (\Delta T_{th} a_i^2/b)^{1/2}$ by

$$J_{max} = J_0(a_i)\left[1 - \frac{1-R^2}{R\sinh(a_i L/2) + \cosh(a_i L/2)}\right]^{-1/2} . \qquad (3)$$

The dependence on $L$ is somewhat complex, and to simply matters, we consider two limits of $J_{max}$ as a function of $L$.

(i) Short CNF ($a_i L/2 << 1$) with any $R$:

$$J_{max} \sim J_0(a_i)\sqrt{\frac{8(1-R^2)}{4Ra_iL + (a_iL)^2}} . \qquad (4)$$

(ii) Long CNF ($a_i L/2 >> 1$) with any $R$:

$$J_{max} \sim J_0(a_i)\left[1 + (1-R)\exp(\frac{-a_iL}{2})\right] . \qquad (5)$$

Depending on $R$, $J_{max}$ behaves as $L^{-1/2}$ ($R >> a_iL$) or $L^{-1}$ ($R << a_iL$) in the short-$L$ limit. The long-$L$ limit represents the direct balance of heat generation with dissipation to the substrate, and the exponential factor provides finite $L$ correction. To examine this further, calculated results for $\Delta T(x)$ and $a(x)$ are shown in Fig. 3(a), which corresponds to case 1 in Fig. 2. Limit (i) was discussed in our previous work [11], and limit (iii) was reported elsewhere [7].

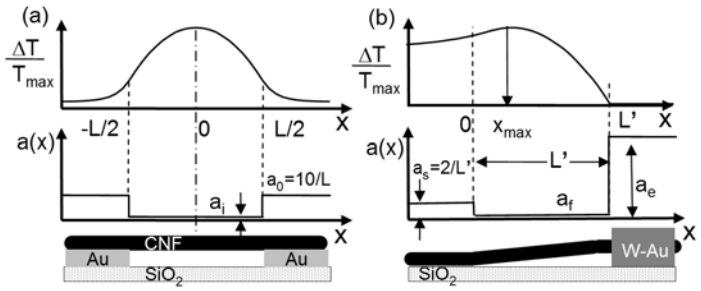


Fig. 3. (a) Model for symmetric contacts with discrete dissipation factors $a_i$ and $a_0$. $\Delta T$ solution in Section II.*A* is plotted for $a_0 L = 10 >> a_i L$. (b) Model for asymmetric contacts with dissipation factors $a_s$, $a_f$, and $a_e$. $\Delta T$ solution in II.*B* is plotted with $a_e L' >> a_s L' = 2.5\ \mu m^{-1} \times 0.8\ \mu m = 2.0 >> a_f L'$.

### *B. Breakdown Location for Asymmetric Contacts*

We consider for the $SiO_2$ region $x < 0$ and $a(x) = a_s$, for the fully suspended ($S = 0$) region $0 < x < L'$, $a(x) = a_f$, and for the electrode region $L' < x$, $a(x) = a_e$, as indicated in Fig. 3(b), where $a_s$, $a_f$, and $a_e$ are defined. In the limit of very large $a_e$ due to the W-Au electrode, finite $a_s$ due to the $SiO_2$-supported region, and negligible $a_f$ in the suspended segment, we obtain an approximated expression for $x_{max}$,

$$x_{max} \cong \left[\frac{1}{2} - \frac{1}{(a_s L')^2}\right] L' . \qquad (6)$$

The breakdown location clearly shifts away from the midpoint by $1/(a_s L')^2$ toward the $SiO_2$-supported region, since the heat dissipation in the W-Au region is much more efficient than the $SiO_2$-supported region. This result is shown in Fig. 3(b), where $\Delta T_{max}$ shifts away from the W-Au contact with $\Delta T \sim 0$ there, and remains finite near the $SiO_2$-supported region. This prediction is completely consistent with our SEM observations shown in Fig. 2, as discussed below.

## III. COMPARISON WITH EXPERIMENT

In Fig. 1, there is a straight-line lower bound for the $J_{max}$ versus $1/L$ behavior, and its gradient is $(8\Delta T_{th}/b)^{1/2} = 54$ kA/m from (4) in the limit of negligible heat dissipation between electrodes $R << a_i L$, which is expected to be the case for entirely suspended cases with $S = 0$. Thus, $\Delta T_{th}/b = \Delta T_{th}\kappa\sigma = 3.4 \times 10^8$ W/Ωm$^2$. We do not have direct measurement results for $\Delta T_{th}$ and

κ. For carbon nanofibers, a value of σ = 24 kS/m was reported based on four-point measurement [8]. Our CNF samples yield σ = $10^4$ ~ $10^5$ S/m with an average of 25 kS/m, obtained using four-point measurement. For carbon nanotubes, $\Delta T_{th}$ was estimated to be 600 K in air through thermo-gravimetric measurement [15]. κ = 12 W/m-K was deduced from thermal resistance measurement using Pt-coated carbon nanofiber [17]. If $\Delta T_{th}$ = 600 K and κ = 12 W/m-K are used, then σ = 47 kS/m, which is double the reported value as well as our average value, but still within our measured σ range. Fabris *et al.* [14] pointed out that the $\Delta T_{th}\kappa\sigma$ product tends to be overestimated without considering heating at electrode contacts in the model. This would explain our somewhat large $\Delta T_{th}\kappa\sigma$ value extracted from the measurement data in Fig. 1.

From $(8\Delta T_{th}/b)^{1/2}$ = 54 kA/m, we deduce the long-$L$ limit for $J_{max}$, $J_0(a_i) = (\Delta T_{th} a_i^2/b)^{1/2}$ = 19 (kA/m) × $a_i$ ($m^{-1}$). Fitting this to measurement results in Fig. 1 for $S$ = 0.69, 0.81, and 1.0 and using (4) in the limit $R$ <<1, we obtain $a_i$ = 2.48, 1.60, and 1.27 $\mu m^{-1}$, with $J_0$ = 4.5, 3.0, and 2.3 MA/$cm^2$, respectively. As shown in Fig. 1, the resulting calculated $J_{max}$ behaviors compare well with measurement results for substrate-supported cases.

Breakdown locations in Fig. 3 can be explained by assuming $a \rightarrow \infty$ for W-Au contacts, $a \sim 0$ for full suspension, and finite $a$ for Au and $SiO_2$ contacts. Applying these assumptions for symmetric contacts leads to breakdown location at the midpoint of the suspended segment. This prediction is confirmed by the observations shown in Fig. 2(a) and (b). For case 3 in Fig. 2(c), since the W-Au contact can dissipate heat much more effectively, the breakdown location moves away from the center towards the $SiO_2$-supported region. In fact, the observed breakdown location $x_{max}/L'$ in Fig. 2(c) is shifted by ~1/4 from the center towards the substrate contact. Using (6) with $L'$ ~ 0.8 μm, we estimate $a_s$ ~ 2.5 $\mu m^{-1}$. This indicates that the breakdown experiments and the results of the present model can be used for estimation of the heat dissipation factor in these hybrid substrate contact systems. A calculated $\Delta T/T_{max}$ plot corresponding to these values is shown in Fig. 3(b). $\Delta T$ is clearly non-zero in the $SiO_2$-supported region, and its peak is shifted toward this region away from the W-Au contact. This prediction matches well the observation in Fig. 2(c). Based on this analysis, one can study heat dissipation in similar systems by examining breakdown locations experimentally.

## CONCLUSION

We have developed an analytical heat transfer model taking into account a piecewise spatially varying heat dissipation factor in the carbon nanofiber interconnect applications and successfully explain previous measurements of current capacity and observations of breakdown locations under various electrode and substrate-supported contact conditions.

## ACKNOWLEDGMENT

This work was supported by the United States Army Space and Missile Defense Command SMDC and carries Distribution Statement A, approved for public release, distribution unlimited.

## REFERENCES

[1] M. Nihei, A. Kawabata, D. Kondo, M. Horibe, S. Sato, and Y. Awano, "Electrical properties of carbon nanotube bundles for future via interconnects," *Jpn. J. Appl. Phys.*, vol. 44,, pp.1626-1628 (2005).

[2] S. Salahuddin, M. Lundstrom, and S. Datta, "Transport effects on signal propagation in quantum wires," *IEEE Trans. Electron Devices*, vol. 52 (8), pp.1734-1742 (2005).

[3] J. J. Plombon, K. P. O'Brien, F. Gstrein, V. M. Dubin, and Y. Jiao, "High-frequency transport electrical properties of individual and bundled carbon nanotubes," *Appl. Phys. Lett.*, vol. 90 (6), p.063106 (2007).

[4] P. J. Burke, "An RF circuit model for carbon nanotubes," IEEE Trans. on Nanotechnology, vol. 2 (1), pp.55-58 (2003).

[5] M. A. Kuroda, A. Cangellaris, and J.-P. Leburton, "Nonlinear transport and heat dissipation in metallic carbon nanotubes," *Phys. Rev. Lett.*, vol. 95 (26), p.266803 (2005).

[6] E. Pop, D. Mann, K. Goodson, and H. Dai, "Electrical and thermal transport in metallic single-wall carbon nanotubes on insulating substrates, *J. Appl. Phys.*, vol. 101 (9), p.093710 (2007).

[7] C. Durkan, M. A. Schneider, and M. E. Welland, "Analysis of failure mechanisms in electrically stressed Au nanowires," *J. Appl. Phys.*, vol. 86 (3), pp.1280-1286 (1999).

[8] L. Zhang, D. Austin, V. I. Merkulov, A. V. Meleshko, K. L. Klein, M. A. Guillorn, D. H. Lowndes, and M. L. Simpson, "Four-probe charge transport measurements on individual vertically aligned carbon nanofibers," *Appl. Phys. Lett.* vol. 84 (20), pp.3972-3974 (2004).

[9] Q. Ngo, A. M. Cassell, A. J. Austin, J. Li, S. Krishnan, M. Meyyappan, and C. Y. Yang, "Characteristics of aligned carbon nanofibers for Interconnect Via applications," *IEEE. Elec. Dev. Lett.*, vol. 27 (4), pp.221-224 (2006).

[10] M. Suzuki. Y. Ominami, Q. Ngo, C. Y, Yang, A. Cassell, and J. Li, "Current induced breakdown of carbon nanofibers," *J. Appl. Phys.* vol. 101 (11), p.114307 (2007). In Figs. 2 and 3, high resolution images of CNFs and breakdown locations are shown.

[11] H. Kitsuki, T. Yamada, D. Fabris, J. R. Jameson, P. Wilhite, M. Suzuki, and C. Y. Yang, , "Length dependence of current-induced breakdown of carbon nanofibers," *App. Phys. Lett.*, vol. 92 (17), p.173110 (2008).

[12] T. Saito, T. Yamada, D. Fabris, H. Kitsuki, P. Wilhite, M. Suzuki, and C. Y. Yang, "Improved contact for thermal and electrical transport in carbon nanofiber interconnects," *Appl. Phys. Lett*. vol. 93 (10), p.102108 (2008).

[13] M. Suzuki, T. Yamada, and C. Y. Yang, "Monte Carlo simulation of scanning electron microscopy bright contrast images of suspended carbon nanofibers," *Appl. Phys. Lett.* vol. 90 (8), p.083111 (2007).

[14] D. Fabris, H. Kitsuki, T. Yamada, X. Sun, J. Gonzalez-Cruz, and C. Y. Yang, "Temperature modeling for carbon nanofiber breakdown," in the Proceedings of *2008 ASME Summer Heat Transfer Conference*, Aug. pp.10-14, Jacksonville, FL.

[15] K. Hata, D. N. Futaba, K. Mizuno, T. Namai, M. Yumura, and S. Iijima, "Water-assisted highly efficient synthesis of impurity-free single walled carbon nanotubes," *Science*, vol. 306, pp.1362-1364 (2004).

[16] T. Yamada, T. Saito, D. Fabris, and C. Y. Yang, "Electrothermal Analysis of Breakdown in Carbon Nanofiber Interconnects," *IEEE Elec. Dev. Lett.* vol. 30 (5), pp.469-471 (2009).

[17] C. Yu, S. Saha, J. Zhou, L. Shi, A. M. Cassell, B. A. Cruden, Q. Ngo, and J. Li, "Thermal contact resistance and thermal conductivity of carbon nanofibers," *J. Heat Transfer*, vol. 128, pp. 234-239 (2006).